A new time and space resolved transmission spectrometer for research in inertial confinement fusion and radiation source development

P. F. Knapp, C. Ball, K. Austin, S. B. Hansen, M. D. Kernaghan, P. W. Lake,
D. J. Ampleford, L. A. McPherson, D. Sandoval, P. Gard, M. Wu, C. Bourdon,
G. A. Rochau, R. D. McBride,[a] and D. B. Sinars
Sandia National Laboratories, Albuquerque, New Mexico 87185, USA

We describe the design and function of a new time and space resolved x-ray spectrometer for use in Z-pinch inertial confinement fusion and radiation source development experiments. The spectrometer is designed to measure x-rays in the range of 0.5–1.5 Å (8–25 keV) with a spectral resolution $\lambda/\Delta\lambda \sim 400$. The purpose of this spectrometer is to measure the time- and one-dimensional space-dependent electron temperature and density during stagnation. These relatively high photon energies are required to escape the dense plasma created at stagnation and to obtain sensitivity to electron temperatures $\gtrsim 3$ keV. The spectrometer is of the Cauchois type, employing a large 30×36 mm^2, transmissive quartz optic for which a novel solid beryllium holder was designed. The performance of the crystal was verified using offline tests, and the integrated system was tested using experiments on the Z pulsed power accelerator. *Published by AIP Publishing.* [http://dx.doi.org/10.1063/1.4973914]

I. INTRODUCTION

In high energy density physics research, x-ray spectroscopy is a fundamental tool used to probe plasma conditions. As temperatures and densities are pushed ever higher, it is necessary for instruments to measure commensurately higher photon energies in order to diagnose experiments. As an example, K-shell spectroscopy is a common technique used to measure electron temperature and density.[1,2] This technique requires an element to be ionized into the K-shell (i.e., He- or H-like). Argon, which emits characteristic radiation in the vicinity of 4 Å has been used extensively as a dopant in Inertial Confinement Fusion (ICF) research because it ionizes into the K-shell at temperatures ~ 1 keV.[3–5] However, at higher temperatures ($\gtrsim 3$ keV), argon is no longer a sensitive thermometer. To probe the plasma at these conditions, it is necessary to use higher Z elements, which emit diagnostically useful radiation at shorter wavelengths. For this reason, a useful dopant for recent gas-filled (e.g., non-cryogenic) ICF experiments is Kr with the He-α resonance line sitting at ≈ 0.96 Å.[2,6,7] Alternatively, at the National Ignition Facility, plastic capsules are doped with germanium.[8] As the shell material mixes into the hotspot, the Ge dopant will emit radiation at ≈ 1.2 Å providing a signature of fuel/shell mix as well as a probe of hot-spot conditions.

Additionally, in the quest to develop efficient radiation sources for Radiation Effects Sciences (RES), it is desired to push to higher photon energies and flux. For these sources and their applications, it is important to understand both the time history of the line radiation and the time evolution of the source conditions. Z-pinch radiation sources can be modified in myriad ways to enhance the thermal radiation output as well as non-thermal radiation. Understanding the evolution of the pinch and where and when these different sources occur is crucial to optimizing them for output.

In this manuscript, we report on the design, characterization, and construction of a time-resolved, high energy spectrometer for use in diagnosing ICF and RES experiments on the 26 MA Z pulsed power generator at Sandia National Laboratories.[9] This spectrometer, referred to as the Time Gated High Energy Radiation (TiGHER) spectrometer, is a Cauchois type transmission spectrometer[10,11] sensitive to the 0.5–1.5 Å wavelength range. It consists of an array of imaging slits, a transmissive quartz dispersion element, and a microchannel plate (MCP) detector for time resolution. In Sec. II, we discuss the design of the instrument including the dispersion and resolution (Sec. II A), unique features of the crystal holder (Sec. II B), and techniques employed for shielding from debris and hard x-ray background (Sec. II C). In Sec. III, we discuss the results of characterization tests as well as preliminary results from Z experiments. Finally, in Sec. IV, we summarize the instrument design and future improvements that are being considered.

II. SPECTROMETER

A. Calculated performance

The spectral range is determined by the elements considered to be diagnostically useful for ICF plasmas reaching $T_e \gtrsim 3$ keV or that are interesting for RES purposes. The Cauchois geometry was chosen because of the ample experience with using the Compact Rugged In-chamber TRansmission (CRITR) spectrometer at the Z facility,[12] which is a time integrated instrument similar to TiGHER. It was determined that a spectral resolving power $\lambda/\Delta\lambda \gtrsim 300$ was required, with $\lambda/\Delta\lambda \sim 500$ being desirable, in order to diagnose electron temperatures using the line ratios in the He-α complex (e.g.,

---

Li-like to He-like). With a given detector resolution, this information is sufficient to design an instrument capable of meeting these goals.

Because of the mature technology of the Gen II MCP developed at Sandia National Laboratories in conjunction with NSTec,[13,14] we chose to use this detector. These cameras have 8 independently gated strips, each with 4 mm height and 40 mm length. They are designed to have a uniform gain profile across the entire strip, which is necessary for quantitative spectroscopy applications. They can be gated with a minimum gate width of ≈200 ps. Testing at 15 keV photon energy (0.82 Å) indicates that the camera has a resolution of ≈50 μm.[15] The use of a cylindrically bent quartz $10\bar{1}1$ crystal with a 250 mm radius of curvature provides sufficient dispersion to achieve the desired resolution over most of the spectral ranges. This makes TiGHER almost identical to CRITR, except that the crystal is rotated to 8.5° instead of 10° as used in CRITR. This slight change in angle was chosen such that the Kr He-α line appears on the detector at the Rowland circle where the spectral lines are in focus.[11] Since the detector is flat, this can only be achieved for a single photon energy. The Kr line was chosen because it is nearly in the center of the spectral range and it is ideally suited for diagnosing ICF plasmas.

The calculated dispersion and resolving power ($\lambda/\Delta\lambda$) are shown in Fig. 1. The resolving power is calculated using the approximation

$$\frac{\lambda}{\Delta\lambda} = \frac{\lambda}{\delta x}\left(\frac{d\lambda}{dx}\right)^{-1}. \tag{1}$$

The spectral dispersion ($d\lambda/dx$) is calculated using ray tracing and is well approximated as a constant function of λ. The spatial resolution, δx, at the detector is assumed to be 50 μm. Under these approximations, the resolving power is $\lambda/\Delta\lambda$ ≈ 650 at 0.96 Å, exceeding the requirement. At higher photon energies, the resolution is degraded somewhat.

A slit is used in front of the spectrometer to provide spatial resolution along the axis of the pinch. The 4 mm height of each strip, along with the geometry of the Z chamber, led us to design two different magnifications. The magnification is defined as $M = x_{ss}/x_{sd}$, where x_{ss} and x_{sd} are the source-to-slit distance and the slit-to detector distance along the principle ray. Since the slit-to-detector distance is fixed, changing the magnification is accomplished simply by
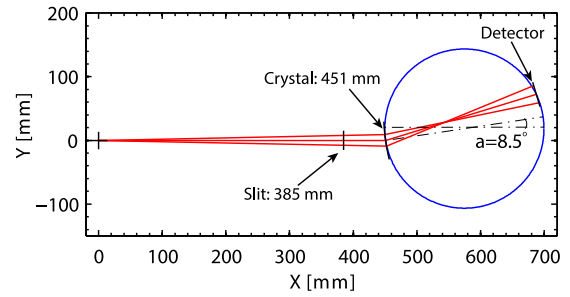
FIG. 2. Schematic of the TiGHER spectrometer showing the locations and relative orientations of the slit, crystal, and detector. Three rays are traced through the system (red lines), showing the full data path.

moving the instrument further back in the Z chamber. For small or suitably apertured loads, a 0.8 magnification option is available. For taller loads, such as wire arrays and gas puffs, a 0.5 magnification configuration is available. A schematic view of the 0.8 magnification configuration is shown in Fig. 2.

Assuming the use of a 50 μm slit and considering the 50 μm detector resolution, we can calculate the spatial resolution in the target plane. The geometric resolution is given as

$$R_g \approx w(1 + 1/M), \tag{2}$$

where w is the slit width. We can assume that due to the high photon energies involved and the relatively large slit width, that diffraction is negligible. If we assume that the geometric resolution represents the Full Width at Half Maximum (FWHM) of a gaussian line spread function and the detector resolution is also well represented as a gaussian, we can add the contributions in quadrature giving a spatial resolution of ≈120 μm and ≈160 μm for the 0.8 magnification and 0.5 magnification configurations, respectively. The dominant source of axial variations in most Z-pinch experiments is the Magneto-Rayleigh-Taylor (MRT) instability, which cascades to relatively large wavelengths (~500 μm) at stagnation.[16] Therefore this resolution is adequate to capture axial variations dominated by this effect.

B. Components

The entire instrument is shown in Fig. 3(a). There are four main components to the spectrometer: the slit array, crystal, detector, and alignment system. The slit array is a fairly straightforward array of 8 slits backed by a baffle to provide structural integrity. The slits are each machined into a solid piece of 125 μm thick tantalum. Standard available slits are 50 or 100 μm wide. The baffle plate has 8, 1.25 mm wide slits machined into a 2 mm thick stainless steel plate. The slits are mounted onto the baffle for mechanical stability and then placed in the mount using precision pins for alignment.

Because of the need to image 8 slits onto a ≈40 mm × 40 mm detector, the crystal must be much larger than that used in CRITR. A single piece of quartz cut to 30 mm wide × 36 mm tall × 0.1 mm thick is used. Because of the large size, we designed a crystal holder that pinches the crystal between two solid pieces of Be machined to the desired shape. The total thickness of the assembly (i.e., front Be substrate plus
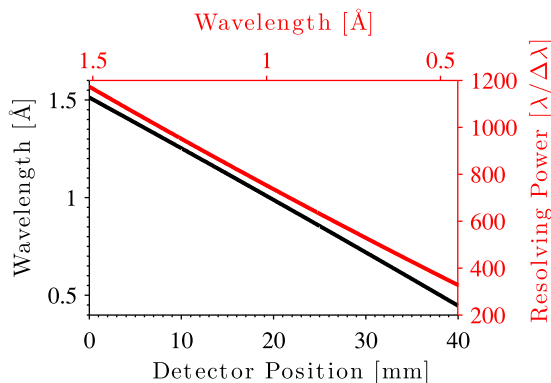

FIG. 1. Wavelength in Angstroms as a function of detector position (black line) and spectral resolution as a function of wavelength (red line). Spectral resolution is calculated assuming a detector spatial resolution of 50 μm.
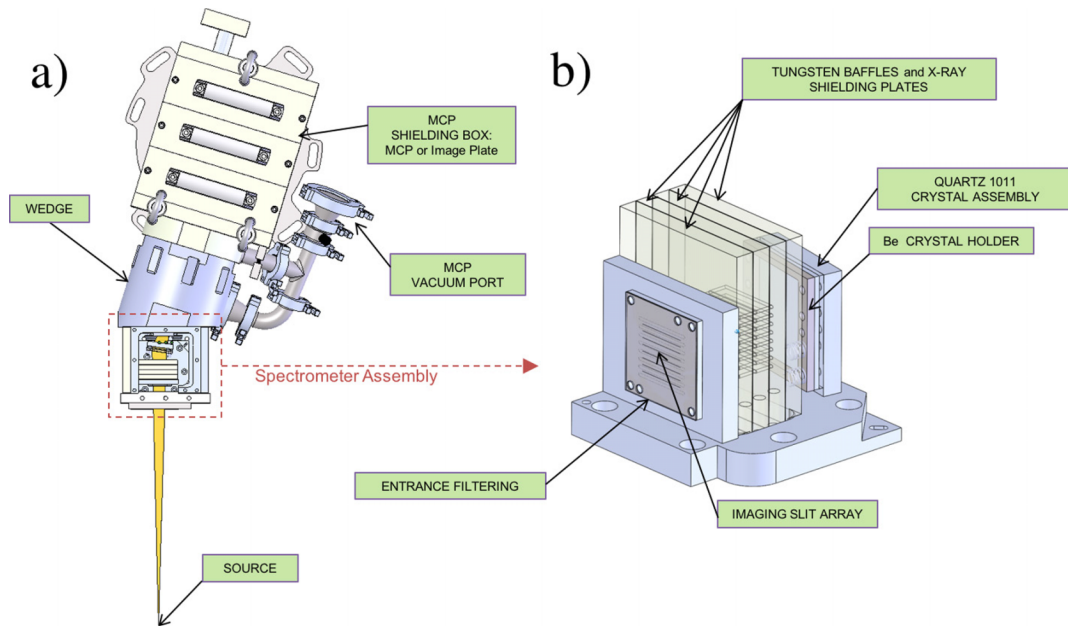
FIG. 3. (a) Top down view of the full TiGHER assembly highlighting the main components. (b) Model drawing of the slit/crystal assembly with tungsten baffling shown. Entrance filtering is placed in front of the imaging slits.

crystal plus back Be substrate) is 5 mm. This holds the shape of the crystal at all points on its surface, in contrast to a hollow frame that would only hold the crystal at its edges, while still allowing the x-rays to pass through relatively unattenuated.

To ensure that the slits are held at precisely the correct angle with respect to the crystal, we have chosen to machine the crystal assembly holder and the slit assembly holder out of a single piece of aluminum, shown in Fig. 3(b). This allows the crystal and slits to be precisely aligned with respect to each other, with no error introduced when components are removed and refurbished. Three tungsten baffle plates are placed in between the slits and the crystal holder to provide additional x-ray shielding and protect the crystal from large pieces of debris. This assembly is located in the spectrometer box using precision alignment pins.

A precision laser alignment system has been designed to ensure that the optical axis of the crystal assembly is aligned to the optical axis of the box. A laser fixture that fits in the spectrometer box with the same alignment pins as the crystal assembly is aligned on an optical bench to fix the laser path to the axis of the instrument. The crystal assembly is removed from TiGHER, and the laser alignment fixture is installed. The laser beam is then used to align the instrument to the desired location on the target, and the instrument is locked in place. Then, the fixture is removed, and the crystal assembly is reinstalled. This process has been verified to produce adequate alignment and reproducibility.

As stated previously, the detector is a Gen II MCP. Optical film is used to record the output of the phosphor. The use of film is required in the Z vacuum chamber due to the extremely harsh electrical environment. The camera requires 8 high bandwidth signal cables and two bias cables to be routed into the Z vacuum chamber. These cables and their connections are protected with steel shielding at the vacuum chamber wall and are hidden inside the tungsten shielding box built for the camera. The spectrometer assembly containing the crystal and slits is connected to the camera by a "wedge," as shown in Fig. 3(a). This wedge maintains the correct orientation and separation between the crystal and the detector. New spectrometer configurations can be made simply by fabricating a new wedge.

The MCP requires its own vacuum system separate from the Z chamber. The MCP is ideally operated at a pressure of $\lesssim 1 \times 10^{-5}$ Torr. While the Z chamber can reach this level, it also experiences a large pressure pulse and distributes soot after the experiment which could damage the MCP. Through testing, it was determined that the use of an isolation filter between the Z environment and the MCP would not allow for sufficiently low pressure to be reached at the MCP surface in a reasonable amount of time to complete an experiment. Additionally, this method would require that the MCP be exposed to atmosphere on a routine basis, which would negatively affect its performance characteristics. For these reasons, it was decided to run an independent vacuum line to the MCP itself. This line pumps a small volume immediately in front of the MCP, which is isolated from the rest of the instrument via a thin plastic window.

C. Shielding

Diagnostics fielded inside the Z vacuum chamber are subjected to an extremely harsh environment. Z-pinch loads generate approximately MJ's of soft x-rays, hundreds of kJ's of keV-range x-rays, and hundreds of J's of hard x-rays. Additionally, copious debris is generated during the discharge. As such, all in-chamber diagnostics require heavy armor and high-Z shielding to protect sensitive components and shield against the high energy background.

To protect against the hard x-ray background, the MCP is shielded in all directions by 1 in. of tungsten armor. This

MCP shielding box (Fig. 3(a)) has segmented doors allowing access to the MCP to make connections and engage the film pack. The film pack itself is also made of tungsten to provide additional shielding for the film. Tests were performed on a variety of Z experiments to assess the level of background exposure that the film would experience with and without a phosphor. This approach of shielding the detector on all sides, including the film pack, was determined to be necessary to keep the background to an acceptable level. The use of thick tungsten x-ray shielding also provides excellent debris mitigation. Penetrations into the tungsten are required for electrical cables, vacuum pumping, and the spectrometer data path. Wherever possible, these penetrations are made with at least one 90° turn to mitigate scattering of high energy photons into the vicinity of the MCP.

The front end of the spectrometer is the most vulnerable, as it offers 8 openings with a direct line of sight to the load. Previous experience has shown that a total of 1.5 mm of Kapton filtering (3 pieces of 0.5 mm thick Kapton) is sufficient to protect the spectrometer. The first two layers of filtering are routinely destroyed with some damage typically occurring to the third layer. Occasionally, a large piece of debris directly impacts the spectrometer entrance and will do more damage, but this is rare. In these cases, the slits are generally destroyed, but heavy baffling on the slit array protects the internal components from these events.

III. RESULTS

A. Characterization data

The spectrometer was characterized in a time integrated manner on a Manson source to verify the dispersion of the instrument and the quality of the crystal mounting. Figure 4(a) shows a calibration spectrum where a Au anode was used to expose image plate, recording the characteristic L-shell transitions. Then a Y anode was used to expose the same image plate, recording the characteristic $K\alpha$ and $K\beta$ transitions. This procedure gives a large number of well known line positions that can be used to determine the actual spectrometer dispersion. In this image, the edge of the crystal on the low energy side of the detector ($X = 0$ mm) is clearly distorted. Moving to shorter wavelengths, further away from this edge of the crystal, the lines become progressively straighter, until the distortion is barely visible above ~1 Å (the location of the Au $L_{\beta1}$ lines). This distortion is likely due to imperfections in the substrate in the form of local non-uniformities in the radius of curvature. We are exploring ways to improve this through different manufacturing techniques, such as diamond turning. Nevertheless, this can be corrected for in post-processing.

Figure 4(b) shows the positions of four of these known lines on the detector (orange circles) with the error bars showing the 2σ deviation in the line position as a function of height on the detector. This variation is <5% over the entire detector. The blue line shows the wavelength as a function of detector position calculated via ray tracing which is in excellent agreement with the measured line positions. The observed distortion of the spectrum due to the crystal warping at the low energy side makes the usable spectral range slightly
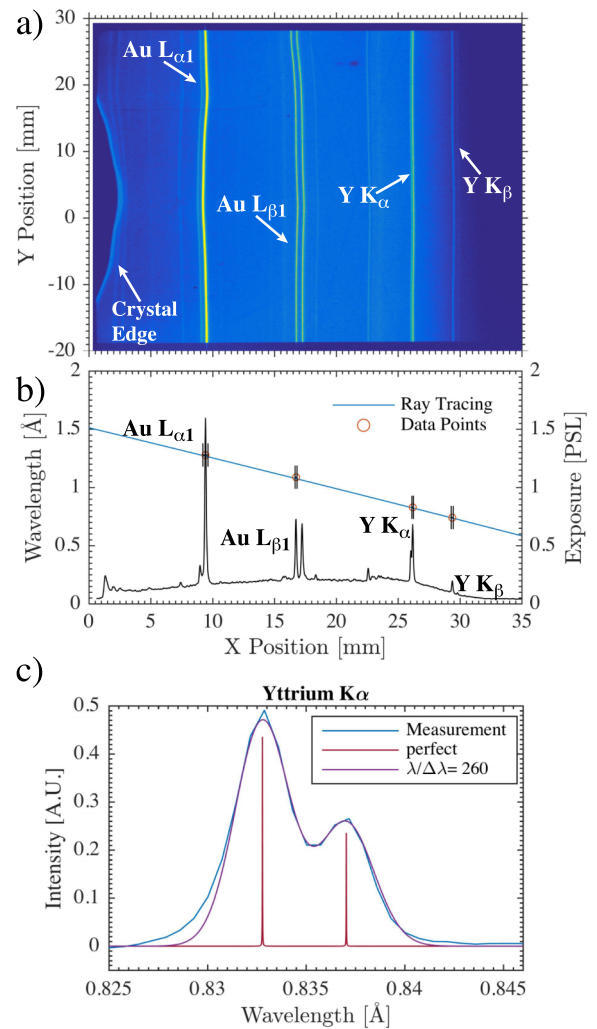

FIG. 4. (a) Cropped portion of a calibration spectrum taken using the Manson source with Au and Y anodes. (b) Orange circles show locations of 4 lines from the image. The blue line shows the wavelength as a function of detector position from the ray tracing calculations. The black line is a line out from the spectrum with the specific spectral features identified. (c) Closeup of the Y $K\alpha$ complex (blue line), two delta functions (red) representing a prefect spectrum, and the result of convolving the perfect spectrum with an instrumental broadening of 3.15 mÅ (purple).

smaller than designed, 0.5–1.4 Å, as opposed to the target of 0.5–1.5 Å. This is a small difference, and it is unlikely to impact the use of this instrument. However, we do believe that this can be corrected with a redesign of the crystal mounting structure.

A rigorous measurement of the spectral resolution is beyond the scope of this paper, but it can be estimated with the available data. First, we must consider the fact that the image plate spatial resolution ($\approx$75 μm) is larger than that of the MCP detector used in the experiment ($\approx$50 μm). Consulting Equation (1), we see that the resolution will appear $\approx$50% worse in the characterization data due to this effect alone. Figure 4(c) shows a closeup of the Yttrium $K\alpha$ complex in blue along with two representative delta functions in red at the nominal locations of the $K\alpha_1$ and $K\alpha_2$ lines. We find a good fit to the data by convolving the delta functions representing a perfect spectrum with a gaussian having a FWHM of 3.15 mÅ. This instrumental broadening corresponds to a

spectral resolution of $\lambda/\Delta\lambda \approx 260$. Applying the correction due to the detector resolution, we find an approximate spectral resolution of ~400 while the calculated curve in Fig. 1 suggests that the spectral resolution should be ~600. The observed degradation in the spectral resolution is likely related to the distortions observed in the spectrum. Non-uniformities in the bend of the crystal will introduce stresses that will act to broaden the crystal rocking curve and, thereby, degrade the spectral resolution. We fully expect that the same efforts required to mitigate the distortions in the spectra will help mitigate the lower than expected resolution.

B. Shot data

In order to test the performance of the instrument in the time-resolved mode, it must be used on a Z shot. Figure 5(a) shows example data from one such test. These data have been corrected for filter transmission, crystal transmission, and for the wavelength dependent crystal reflectivity calculated using the XOP software.[17] In this experiment, a molybdenum wire array was designed to excite non-thermal radiation output at stagnation.[18,19] As such, we expect to see a spectral structure dominated by the Mo $K\alpha$ lines at ≈ 0.73 Å and continuum emission.

The data clearly show emission at the expected photon energy evolving in time from one frame to the next. Additionally, the continuum at the long wavelength side of the image is

seen to evolve in time. Both the line and continuum emission peak in intensity at the same time. The time at which each frame was taken, relative to the peak x-ray power, is shown in the upper left corner of each image. In this experiment, each frame was gated with an 800 ps pulse and separated by 1000 ps. Lineouts from four of the frames are shown in Fig. 5(b). The line emission is not strong enough to discern any changes in the structure of the line as a function of time. However, the $K\alpha_1$ and $K\alpha_2$ lines are resolved, most clearly at $t = 9$ ns, where the emission is the strongest. The data obtained here do not allow a determination of the pinch temperature as a function of time since only the non-thermal emission is observed. However, it demonstrates that data can be obtained in this harsh environment.

IV. CONCLUSIONS AND FUTURE WORK

In summary, we have developed, tested, and fielded a new high-energy, time, and space resolved spectrometer for use in ICF and RES experiments on the Z-machine at Sandia National Laboratories. This instrument uses an 8-frame gated MCP as the time and space resolving detector. Eight slits are used to direct one dimensionally resolved images of the x-ray emission onto each of the independently timed strips. A quartz $10\bar{1}1$ crystal is employed as the transmissive dispersion element. This instrument provides adequate spectral resolution to use the He-α complex of a variety of elements to measure the temperature evolution of z-pinch driven ICF experiments and x-ray sources. The spatial resolution is sufficient to resolve spatial variations smaller than those characteristic of the MRT instability, which tends to dominate these types of experiments at stagnation.

In order to survive the harsh environment in Z and minimize background exposure, the entire camera has been shielded by a minimum of 1 in. of tungsten. This provides excellent debris protection for sensitive components, such as the MCP and high voltage cables. Additionally, the use of tungsten provides adequate shielding from the hard x-ray background typically experienced on Z. Background exposure is still observed in the experimental data with a signal to background ratio of ~3–5, though we believe this can be mitigated by improved instrument design. Internal shielding can be enhanced, particularly at the crossover point between the crystal and the detector. This will help reduce the likelihood of hard radiation being scattered at small angles onto the detector.

We designed a novel crystal mount that sandwiches the flat crystal between two contoured Be components. This provides excellent structural integrity with minimal x-ray attenuation, and it can help to mitigate distortions observed with free standing curved crystals. Some distortion of the crystal is still observed, and we are investigating ways to mitigate this effect. A major benefit of this construction is that the crystal is exceptionally well protected from debris and soot. Since the crystal is not a disposable component, it is then feasible to invest significant resources into calibrating the assembly. Once the crystal warping is mitigated and the resolution is improved, it will then be possible to measure
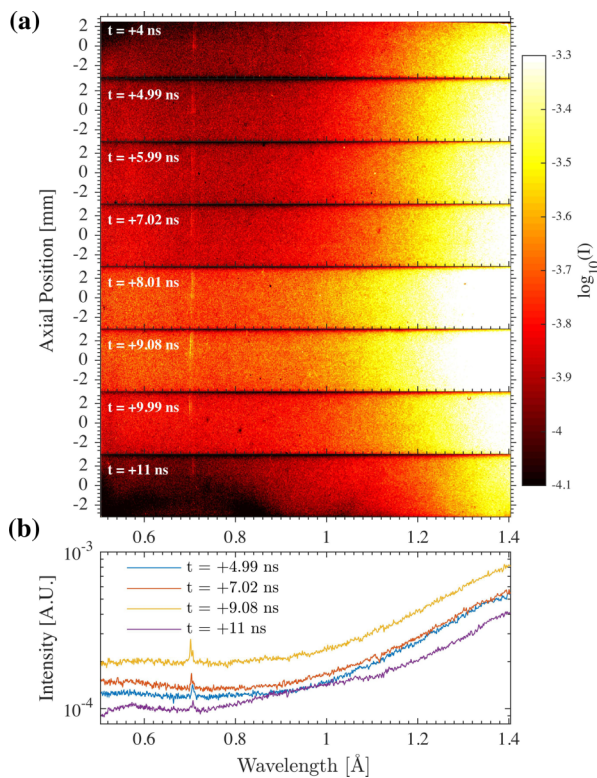

FIG. 5. (a) Data taken on a Mo wire-array experiment, processed to account for crystal reflectivity and filter transmission. 8 frames of data were captured, showing the evolution of emission of the Mo K-α complex at stagnation. Data are shown as the log of the intensity in arbitrary units. Times are relative to peak x-ray power. (b) Lineouts taken at four different times showing the evolution of the Mo K-α lines and the continuum emission.

the reflectivity and spectral resolution of the instrument. We have shown a simple characterization of the dispersion and spatial uniformity. More detailed measurements are underway to better characterize these spatial variations and to develop correction methods.

ACKNOWLEDGMENTS

[1]H. R. Griem, Phys. Fluids B **4**, 2346 (1992).

[2]S. B. Hansen, Phys. Plasmas **19**, 056312 (2012).

[3]S. P. Regan, J. A. Delettrez, R. Epstein, P. A. Jaanimagi, B. Yaakobi, V. A. Smalyuk, F. J. Marshall, D. D. Meyerhofer, W. Seka, D. A. Haynes *et al.*, Phys. Plasmas **9**, 1357 (2002).

[4]D. Sinars, G. Chandler, J. Bailey, R. Mancini, G. Rochau, D. Wenger, R. Adams, M. Adams, H. Scott, A. Faenov *et al.*, J. Quant. Spectrosc. Radiat. Transfer **99**, 595 (2006), Radiative Properties of Hot Dense Matter.

[5]I. Golovkin, R. Mancini, S. Louis, Y. Ochi, K. Fujita, H. Nishimura, H. Shirga, N. Miyanaga, H. Azechi, R. Butzbach *et al.*, Phys. Rev. Lett. **88**, 045002 (2002).

[6]A. R. Miles, H.-K. Chung, R. Heeter, W. Hsing, J. A. Koch, H.-S. Park, H. F. Robey, H. A. Scott, R. Tommasini, J. Frenje *et al.*, Phys. Plasmas **19**, 072702 (2012).

[7]T. Ma, H. Chen, P. K. Patel, M. B. Schneider, M. A. Barrios, D. T. Casey, H.-K. Chung, B. A. Hammel, L. F. Berzak Hopkins, L. C. Jarrott *et al.*, Rev. Sci. Instrum. **87**(11), 11E327 (2016).

[8]S. P. Regan, R. Epstein, B. A. Hammel, L. J. Suter, J. Ralph, H. Scott, M. A. Barrios, D. K. Bradley, D. A. Callahan, C. Cerjan *et al.*, Phys. Plasmas **19**, 056307 (2012).

[9]M. E. Savage, K. R. LeChien, M. R. Lopez, B. S. Stoltzfus, W. A. Stygar, D. S. Artery, J. A. Lott, and P. A. Corcoran, in *2011 IEEE Pulsed Power Conference* (IEEE, 2011), pp. 983–990, ISSN: 2158-4915.

[10]Y. Cauchois, J. Phys. Radium **4**, 61 (1933).

[11]J. F. Seely, L. T. Hudson, G. E. Holland, and A. Henins, Appl. Opt. **47**, 2767 (2008).

[12]D. B. Sinars, D. F. Wenger, S. A. Pikuz, B. Jones, M. Geissel, S. B. Hansen, C. A. Coverdale, D. J. Ampleford, M. E. Cuneo, L. A. McPherson *et al.*, Rev. Sci. Instrum. **82**, 063113 (2011).

[13]C. A. Kruschwitz, M. Wu, K. Moy, and G. Rochau, Rev. Sci. Instrum. **79**(10), 10E911 (2008).

[14]C. A. Kruschwitz, M. Wu, and G. A. Rochau, Rev. Sci. Instrum. **82**, 023102 (2011).

[15]M. Wu, K. Moy, C. Kruschwitz, and G. Rochau, Rev. Sci. Instrum. **85**(11), 11D607 (2014).

[16]R. D. McBride, S. A. Slutz, C. A. Jennings, D. B. Sinars, M. E. Cuneo, M. C. Herrmann, R. W. Lemke, M. R. Martin, R. A. Vesey, K. J. Peterson *et al.*, Phys. Rev. Lett. **109**, 135004 (2012).

[17]M. Sanchez del Rio, C. Ferrero, and V. Mocella, Proc. SPIE **3151**, 312 (1997).

[18]D. J. Ampleford, B. Jones, C. A. Jennings, S. B. Hansen, M. E. Cuneo, A. J. Harvey-Thompson, G. A. Rochau, C. A. Coverdale, A. R. Laspe, T. M. Flanagan *et al.*, Phys. Plasmas **21**, 056708 (2014).

[19]S. B. Hansen, D. J. Ampleford, M. E. Cuneo, N. Ouart, B. Jones, C. A. Jennings, A. Dasgupta, C. A. Coverdale, G. A. Rochau, G. Dunham *et al.*, Phys. Plasmas **21**, 031202 (2014).